Novel mesoporous silica (MCM-41) and its characterization for oil adsorption from produced water injected in water injection projects using fixed bed column processes

Heba H. El-Maghrabi[a], R. Hosny[b,*], M. Ramzi[b], M. Fathy[c]

[a]*Refining Department, Egyptian Petroleum Research Institute (EPRI), 1 Ahmed El-Zomer,*
Nasr City, Box.No. 11727, Cairo, Egypt, Tel. +(202)22747847; Fax: +(202)22747433
[b]*Production Department, Egyptian Petroleum Research Institute (EPRI), 1 Ahmed El-Zomer, Nasr City, Box. No. 11727, Cairo, Egypt,*
Tel. +(202)22747847; Fax: + 202 22747433, emails: dr.rashahosny@yahoo.com (R. Hosny), mahmoudramzi@yahoo.com (M. Ramzi)
[c]*Applications Department, Egyptian Petroleum Research Institute (EPRI), 1 Ahmed El-Zomer,*
Nasr City, Box. No. 11727, Cairo, Egypt, Tel. +(202)22747847; Fax: +(202)22747433

abstract

Produced water is a by-product of oil and gas production. Once produced water is separated from oil (and gas) it is treated and then discharged to surface water or re-injected for either reservoir pressure maintenance or disposal. Here, we prepared mesoporous silica (MCM-41) by simple single step method and characterized by XRD, FTIR, Raman, N_2 adsorption–desorption and TEM. Then, a continuous fixed bed study was carried out using a prepared MCM-41 for oil removal from produced water. The effects of flow rate and bed height on the breakthrough characteristics of the adsorption system were determined. XRD analysis of the silica powder showed complete formation of a single phase mesoporous MCM-41 without contamination of other phases of silica. The maximum removal (70.26%) was achieved for a flow rate of 0.5 mL/min and a bed height of 1.5 mm. Two models Thomas and Yoon–Nelson were applied to predict the breakthrough curves. The results show that Thomas model fitted well the adsorption data with a correlation coefficient (R^2) at different conditions. R^2 values suggested that the suitable model for describing the chemisorption oil on MCM-41 was Thomas model. The model showed that the MCM-41 was suitable adsorbent for oil using fixed bed adsorption.

Keywords: Produced water; Oil adsorption; Models of Thomas and Yoon–Nelson; Breakthrough curves; MCM-41 mesoporous silica

1. Introduction

Treatment and disposal of a large amount of oily produced water are of a considerable economic and environment burden for oil and gas industry. Formation scales and oil dispersed are considered harmful and expensive problem in the oil and gas industry [1]. Chowdhury et al., use the potential of granular-activated carbon (GAC) for treating wastewater contaminated by manganese, Mn(II) cations [2]. The treatment of produced water requires the separation of suspended and dissolved component such as emulsified oil droplets [3]. Treatment and disposal of oily waste water are presently one of the serious environmental problems contributors and reduce formation damage [4]. The major difficulty in disposing of the oily residuals are the emulsified oil droplets, which are sheltered from spontaneous coalescence into larger flocculants, making oil separation by simple gravity a difficult and time-consuming process [5]. Numerous methods have been used to remove residual oil from waste water, such as adsorption, flocculation, electrocoagulation and flotation [6,7]. There are a number of adsorbents used to adsorb residual oil from produced water such as mesoporous solid basis [8]. Chowdhury et al., produced powdered activated carbon (PAC) from agricultural waste [9].

* Corresponding author.

Mesoporous solid bases are extremely desirable in many processes [10], due to their advantages of accelerated mass transport, negligible corrosion, and easy separation. Great progress has been made in mesoporous solid bases in the last decade [11–14]. In addition to their wide applications in the catalytic synthesis of organics and fine chemicals, mesoporous solid bases have also been used in the field of energy and environmental catalysis [15]. Development of mesoporous solid basis is therefore of significant importance from both academic and practical points of view [16,17]. In this paper, we provide the recent advances in MCM-41 materials belonging to the group of mesoporous silica characterized by a hexagonal arrangement of uniform pores and high surface areas. Since their discovery in 1992 [18,19], MCM-41 materials attracted much attention and were investigated in order to apply as adsorbents, supports and catalysts [20–22]. The important feature of these sorbents is the possibility of creating the pore dimensions in a wide range from 2 to even 10 nm [23]. It allows application of the MCM materials for some special purposes when wider pores can improve transport into the inner space of their structure, for instance, in selective adsorption or catalytic reactions with large molecules. The engineering of the porous structure of ordered silica may be realized by changing the synthesis conditions, the composition of reacting mixture and type of organic template to achieve quite new properties [24].

This work is concerned with the study of fixed bed adsorption of oil on MCM-41 from brine water. A novel direct single step synthesis of silica skeleton is conducted. The investigations of mesoporous silica of MCM-41 type of uniform pore sizes are presented. The obtained material is characterized by using different physicochemical methods in order to identify its surface and structure properties. In addition, the adsorption of oil as a standard method is used to evaluate the capacity of the MCM-41 to eliminate organic molecules from water.

The objective of this study is to control, through an experimental evaluation, the fixed-bed adsorption on MCM-41, and to develop on this basis a model can predict the performances and the characteristics of the bed according to the operating conditions (initial concentration, flow rates and bed depth) [25].

2. Experimental

2.1. Materials

MCM-41 was prepared by a direct precipitation synthesis method using cationic surfactant cetyltrimethylammonium bromide (CTAB) as a template and tetraethylorthosilicate (TEOS) as a silicon source and ammonium hydroxide (28%). All chemical reagents were purchased from the Sigma–Aldrich.

A sample of brine water associated with crude oils produced from the Gulf of Suez oil-field was investigated. The water sample was filtered using ashless filter papers (Whatman No. 42) before they were subjected to the analysis. The results are given in Table 1.

2.1.1. Catalysts preparation

MCM-41 was prepared by a direct precipitation synthesis method using cationic surfactant cetyltrimethylammonium bromide (CTAB) as a template and tetraethylorthosilicate (TEOS) as a silicon source in basic conditions. Typically, at 30°C, 16.2 g of CTAB was dissolved into a solution containing 145 mL of deionized water, 8.21 mL of TEOS and 32 mL of 30% NH3 was then added dropwise and stirred vigorously for 12 h for hydrolysis of TEOS. The product obtained was filtered and dried under vacuum at 40°C night over. The samples were annealed at 550°C in air for 4 h to remove the surfactant.

2.2. Catalyst characterization

The X-ray diffraction analysis was carried out using XPert PRO Powder X-ray diffractometer apparatus. The patterns were recorded using CuKa radiation (λ = 0.1541 nm) at a rating of 40 KV, 40 mA and 2θ range from 0.5° to 80° step time 0.4 (s). The formed crystalline phases were identified using the International Center for Diffraction Data (ICDD) database to determine the composition of the prepared nanostructure.

The morphology of adsorbents was investigated by High-Resolution Transmission Electron Microscope (HRTEM) on Model JEM-200CX, JEOL Japan. A small quantity of the required sample was dispersed in 10 ml ethanol then sonicated for 30 min. Few drops of the resulting suspension were placed on a covered copper grid and photographed at an acceleration rate of 200 KV.

The FTIR spectrum in the 4,000–400 cm^{-1} range was recorded for the prepared samples at room temperature by Perkin Elmer spectroscopy (model FT-IR spectrometer, USA). Samples were prepared using the standard KBr pellets.

Raman spectra were recorded on the dispersive Raman microscope (Model Sentera, Bruker, Germany) instrument at laser wavelength 532 nm [doubled Nd:YAG laser (neodymium-doped yttrium aluminum garnet)] and power 10 mW.

The specific surface area was measured from the N2 adsorption-desorption isotherms at liquid nitrogen

Table 1
Extended analysis for brine water sample

Total dissolved solids	244,927.7 mg/l	pH	7.2@ 25°C
Conductivity	23.2 × 10^{-2} mohs/cm@2.7°C	Density	1.15770 g/m @ 60 F
Resistivity	0.04310 ohm-m @ 24.5°C	Specific gravity	1.15885
Salinity	24,4691.7 mg/l	Hardness	18,883.1 mg/l

Constituents	mg/L	Constituents	mg/L
Lithium	5.60	Fluoride	2.20
Sodium	87175.00	Chloride	148298.00
Potassium	0	Bromide	0
Magnesium	569.62	Nitrate	119.00
Calcium	1390.66	Hydroxide	48.00
Iron	4585.51	Carbonate	Nil
Copper	5.30	Bicarbonate	Nil
Barium	Nil	Sulfate	231.80
Strontium	Nil		2497.00

temperature (–196°C) using Quantachrome Nova 3200 S automates gas sorption apparatus. Prior to such measurements, all samples were perfectly degassed at 300°C for 6 h and under vacuum pressure $1.3 \times 10–3$ Pa.

2.3. Fixed-bed kinetic experiment (column adsorption)

A sample of MCM-41 was 0.5, 1.3 and 1.5 gm "wet filled" to the column with length = 20 cm and internal diameter = 1 cm; depicted in more detail by Chatterjee and Schiewer [26,27], yielding an approximate bed height of 0.5, 1 and 1.5 mm. To increase the bed height, two or three identical columns were serially connected. Oil solution (1,000 mg/L, pH 6.5) from a 20 L oily produced water was pumped upward through the column using a peristaltic pump (VWR) with a flow rate of 0.5, 1, or 1.5 mL/min, as measured with a rotameter. Oily produced water samples, obtained with a fraction collector (Gilson FC203B), were analyzed for oily produced water using an AAS (Perkin Elmer). The calculation of q_1 for the fixed bed was performed as described by Chatterjee and Schiewer [26].

2.4 Breakthrough models

2.4.1. Thomas model

The Thomas model is widely used in column performance modeling [28]. Its derivation assumes Langmuir kinetics of adsorption-desorption and no axial dispersion. The expression for the Thomas model for adsorption column is given as Eq. (1) [29]:

$$\frac{C_t}{C_o} = \frac{1}{1+\exp\left[\left(\dfrac{k_{Th}q_e x}{Q}\right) - k_{Th}C_o t\right]} \tag{1}$$

where k_{Th} (mL/min.mg) is the Thomas model constant, q_e (mg/g) is the predicted adsorption capacity, x is mass of adsorbent (g), Q is influent flow rate (mL/min), C_0 is initial solution concentration (mg/L), and C_t is effluent solution concentration (mg/L). The linear form of Thomas model is expressed as Eq. (2):

$$\ln\left(\frac{C_o}{C_t} - 1\right) = \frac{k_{Th}q_e x}{Q} - k_{Th}C_o t \tag{2}$$

2.4.2. Yoon–Nelson model

A simple model originally developed by Yoon and Nelson proposed that the rate of decrease in the probability of adsorption for each adsorbate molecule is proportional to the probability of adsorption of an adsorbate and the probability of breakthrough of the adsorbate. This model is simpler than other models and also requires no data about the characteristics of the system such as the type of adsorbent and the physical properties of the adsorption bed. The Yoon–Nelson equation is expressed as Eq. (3) [30]:

$$\frac{C_t}{C_o - C_t} = \exp(k_{YN}t - \tau k_{YN}) \tag{3}$$

where k_{YN} (L/min) is the rate constant and τ (min) is the time required for 50% adsorbate breakthrough. The linear form of Yoon–Nelson model is expressed as Eq. (4):

$$\ln\frac{C_t}{C_o - C_t} = k_{YN}t - \tau k_{YN}. \tag{4}$$

3. Results and discussion

3.1. Characterization of MCM-41 catalyst

3.1.1. XRD analysis

The mesoporous structure of MCM-41 catalyst was identified by low angle XRD patterns Fig. 1. The intense diffraction peaks of MCM-41 have a strong peak at $2\theta = 2°–3°$ and two weak peaks at 3°–5° corresponding to the (1 0 0), (1 1 0) and (2 0 0) reflections of hexagonal mesoporous structure, respectively. The d value of the (100) reflection is 38.3 Å, corresponding to a lattice constant of $\alpha = 44.2$ Å.

3.1.2. FT-IR analysis

Fourier transforms infrared spectra (FT-IR) can provide evidence for the frame work of mesoporous MCM-41. In MCM-41 sample Fig. 2 shows the strong FT-IR band observed at 3,460 cm⁻¹ and the broadband at 1,631 cm⁻¹ are due to O–H stretching and H–O–H bending vibrations, respectively [31]. FT-IR bands are observed at around 1,088 and 808 cm⁻¹,
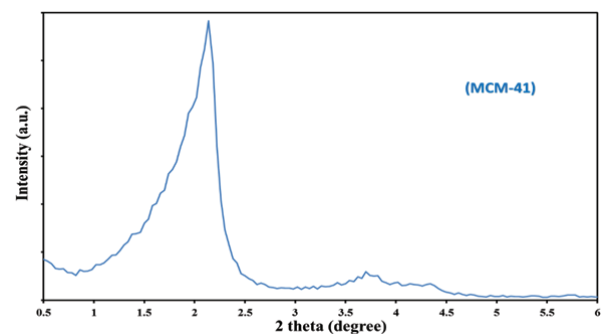

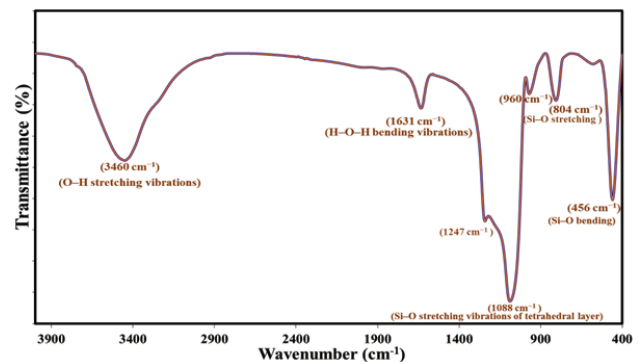Fig. 1. The low angle XRD patterns of mesoporous silica MCM-41.

Fig. 2. FTIR spectrum of prepared MCM-41.

assigned to asymmetric and symmetric Si–O stretching vibrations, respectively [32–35]. The band at around 960 cm^{-1} can be assigned to the lattice defect of the MCM-41 framework. The bands at 545 and 456 cm^{-1} are due to Si–O asymmetric and symmetric bending vibrations, respectively.

3.1.3. Raman analysis

Raman spectroscopy is recognized as a very powerful tool for the identification the surface of mesoporous materials. The Raman spectra of MCM-41 are illustrated in Fig. 3, The MCM-41 sample exhibits four Raman bands at 469, 602, 815, and 963 cm^{-1} where the bands at 469 and 602 cm^{-1} are assigned to the symmetric and asymmetric bending vibration of the Si–O bond, respectively, [32] while the band at 815 cm^{-1} corresponds to the vibration mode of siloxane bridges (an inter-tetrahedral Si–O–Si bending vibration mode). The band at 963 cm^{-1} is attributed to the Si–O–H bond that is directly related to the framework defects, such as surface silanol groups.

3.1.4. Surface structure properties

The mesoporous nature of MCM-41 sample was also confirmed by nitrogen adsorption–desorption isotherm. The reversible type IV isotherm pattern representative of mesoporous materials with distinct capillary condensation step is observed as shown in Fig. 4. As the relative pressure increases, the isotherm exhibits an inflection characteristic of capillary condensation/evaporation steps appear within the mesopores (P/P° = 0.2–0.4), suggesting the sample possess well-ordered regular pore structure. The presence of step increase at P/P° above 0.9 is due to the micropore filling produced by inter-particle spacing. The data of BET surface area and pore volume of prepared MCM-41 can be illustrated in Table 2.

3.1.5. Transmission electron microscope (TEM)

As evidenced by HRTEM image shown in Fig. 5, MCM-41 possesses an order of mesoporous structure. As revealed in the figure, a regular hexagonal array of uniform channels is exhibited indicating a highly ordered pore structure of MCM-41.

3.2. Isothermal study

Two most common isotherm models were employed for describing the adsorption data, which were Langmuir and
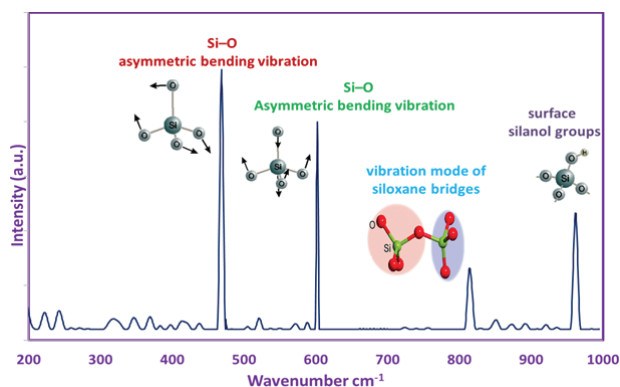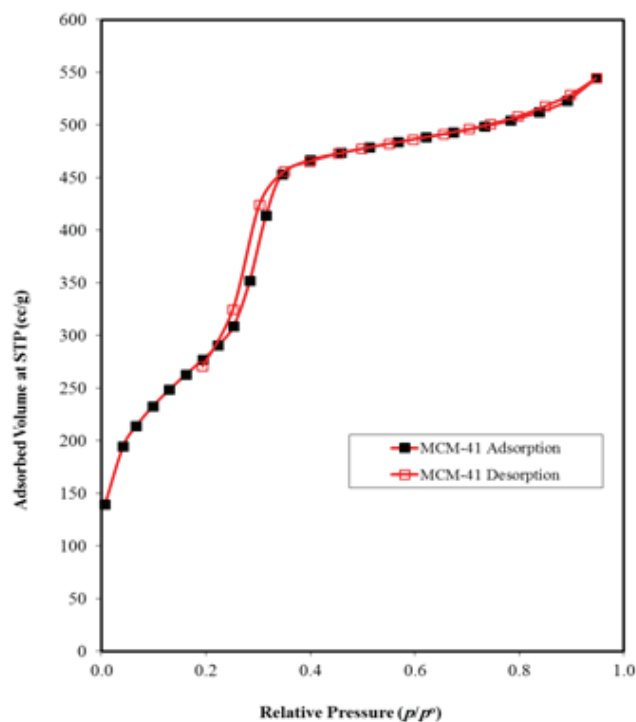

Fig. 4. N2 adsorption–desorption isotherm for MCM-41.

Table 2
Data of BET surface area

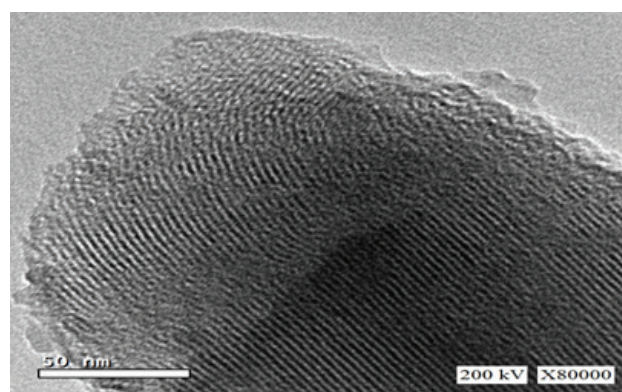| Sample	C_{constant}	S_{BET} (m^2/gm)	V_m (cc/gm)
MCM-41	98.7	1022.6	0.99

Fig. 5. HRTEM image of prepared MCM-41.

Freundlich isotherm. Langmuir equation is based on several assumptions: (i) the adsorbent surface is homogeneous; (ii) there is no interaction between adsorbates in the plane of the surface and (iii) monolayer type of adsorption [36]. The Langmuir equation can be represented in the form of following equations.

$$C_{eq}/Q_{eq} = 1/Q_{mb} + C_{eq}/Q_m \tag{5}$$

Fig. 3. Raman spectrum of prepared MCM-41.

where C_{eq} is the equilibrium concentration of oil in solution (mg/L), Q_{eq} is the amount of oil adsorbed; Q_m and b are Langmuir constants related to adsorption efficiency and energy of adsorption, respectively. The linear plots of C_{eq}/Q_{eq} vs. C_{eq} suggest the applicability of the Langmuir isotherms Fig. 6. The values of Q_m and b were calculated from slope and intercepts of the plots are listed in Table 3. From the results, the values can conclude that the maximum adsorption of adsorbate molecules on adsorbent surface with constant energy and no diffusion of adsorbate in plane of the adsorbent surface. To confirm the favorability of the adsorption process the values were established to be between 0 and 1 and confirm that the ongoing adsorption process is favorable.

The Freundlich isotherm is commonly expressed by the following equation.

$$\log Q_e = \log K_f + 1/n \log C_e \tag{6}$$

where Qe is the amount of oil adsorbed (mg/g), Ce is the equilibrium concentration of oil in solution (mg/L), and Kf and n are constant integrates, the factors affecting the adsorption capacity and intensity of adsorption, respectively. Linear plots of log Qe vs. log Ce shows that the adsorption of oil obeys the Freundlich adsorption isotherm. In Fig. 7, the Freundlich adsorption isotherm obtained by plotting Ce/qe vs. Ce for the adsorption of oil on MCM-41 at the different temperatures investigated, respectively. The Kf and n values are given in Table 3, which indicates that the increase of negative charges on the adsorbent surface makes electrostatic force like Vander waal's between the MCM-41 surface and oil. The values clearly indicate the dominance in adsorption capacity. The intensity of adsorption is an indication of the bond energies between oil and adsorbent, and the possibility of physicosorption rather than chemisorptions.

3.3. Column studies

3.3.1. Effect of flow rate

The effect of the flow rate on the adsorption of oil was investigated by varying the flow rate (0.5, 1 and 1.5 mL/min) with a constant adsorbent bed depth of 0.5 mm and the initial oil concentration of 1,000 mg/L, as shown by the breakthrough curve in Fig. 8.

As indicated in this figure, at the lowest flow rate of 0.5 mL/min, relatively higher uptake values were observed. At higher flow rates (1 and 1.5 mL/min), the breakthrough occurred faster and the breakpoint time and total adsorbed quantity decreased. This behavior can be explained by
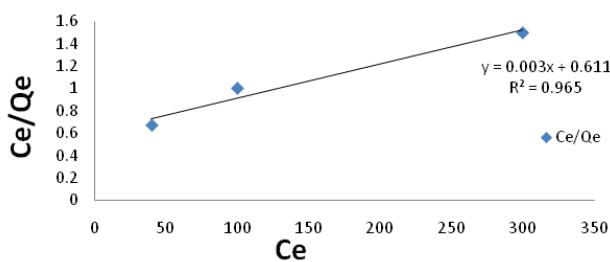
insufficient residence time of the solute in the column: the residence time decreases with the increase of the flow, that leads to insufficient time for diffusion of the oil into the pores of MCM-41 and limits the number of the available active sites for adsorption, thus reducing the volume of the aqueous solution being treated and the solute left the column before equilibrium occurred. The increase in the flow causes a reduction of the resistance of film in the external transfer which causes an improvement in the kinetics of adsorption [37]. But we should mention that this increase is favorable only until one value of the flow beyond which this external resistance is not anymore limited [38].

3.3.2. Effect of bed height

The adsorption capacities of the column with bed heights of 0.5, 1 and 1.5 mm were tested at a constant flow rate of 0.5 mL/min and oil concentration of 1,000 mg/L. The curves of the breakthrough for oil adsorption on MCM-41 three different bed heights were illustrated in Fig. 9. Increasing the
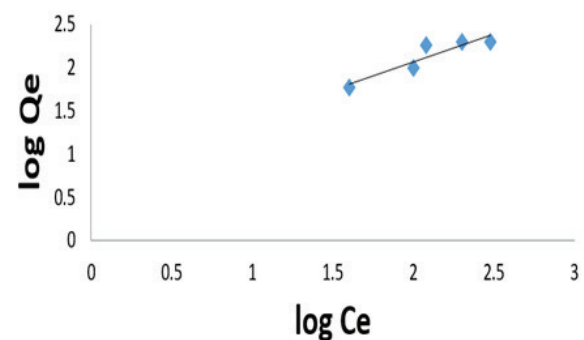
Fig. 7. The Freundlich isotherm for the adsorption of oil onto silica.

Table 3
Langmuir isotherm, Freundlich isotherm results

Langmuir			Freundlich		
K	Q_e	R^2	n	K	R^2
0.004951	930.297	0.982669	1.549759		0.924122

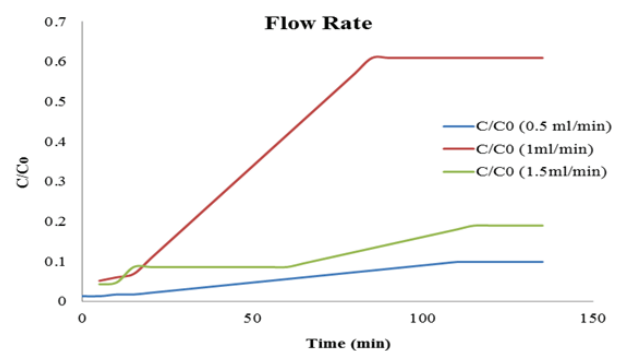Fig. 6. Langmuir isotherm for the adsorption of oil onto silica.

Fig. 8. Flow rate of oil adsorption on MCM-41 vs. time.

height of the bed can be explained by more sites which were supplied for solute so there was increase in the breakthrough time with bed depth [39]. Hence, the breakthrough point of bed height 1.5 mm started at 100 min later than the corresponding bed height 0.5 mm and 1 mm, which explain how large the water volume has been treated using the bed height 1.5 mm.

3.4. Kinetic study of Thomas model

The sorption data at constant oil concentration of 1,000 mg/L and a bed height of 1.5 mm and at three different flow rates of 0.5, 1 and 1.5 mL/min for the sorption process of oil through MCM-41 were applied using Thomas model. The rate constant of Thomas (k_T) (slope) and the bed capacity (the intercept) were calculated from the plotting between
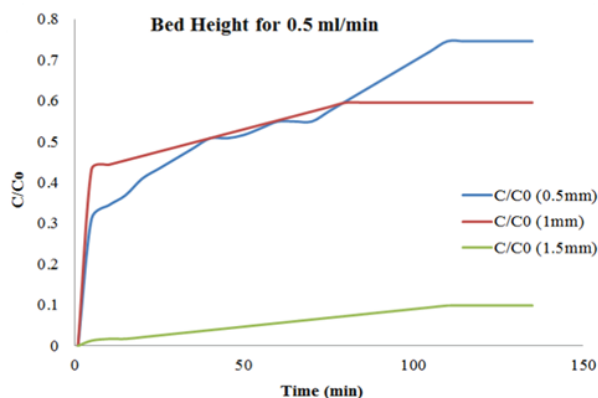
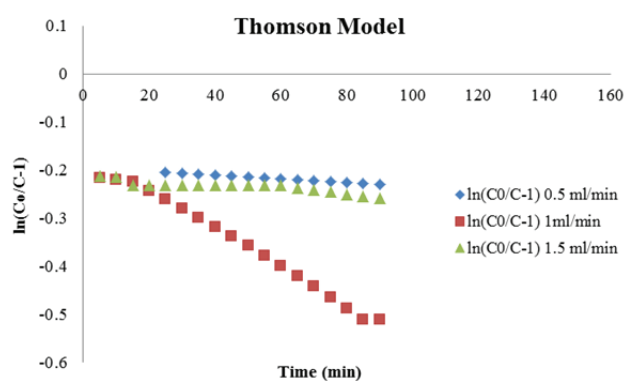Fig. 9. Effect of the bed height for adsorption of oil on MCM-41.

Fig. 10. Thomson model parameters for adsorption of oil on MCM-41.

Table 4
Thomson model parameters

Flow (mL min⁻¹)	k_{Th}	R^2	q (mg g–1)	SSE (%)
0.5	0.000175	0.999994	1113.795	0.001
1	0.00171	0.99585	100.7273	0.002
1.5	0.00017	0.88319	1259.224	0.006

$\ln(C/C_o-1)$ against t at different flow rates as shown in Fig. 10. Values of k_T and q_0 with the regression coefficients are presented in Table 4. *The values of R^2 0.999994, 0.99585 and 0.88319* suggested that the Thomas model was suitable for explaining the chemisorption oil on MCM-41. Table 4 explained that as the flow rate increased from 0.5 to 1.5 mL/min the maximum oil chemisorption capacity increased from 1,113 mg/g to 1,259 mg/g at a constant height of 1.5 m. Fig. 10 shows that there was a good agreement between model predicted values and the experimental points.

3.5. Kinetic study of Yoon–Nelson model

Yoon–Nelson model was applied to the column data obtained from chemisorption with MCM-41, from the plotting of $\ln(C/C_0 - C)$ vs. the time we determined the Yoon–Nelson constant (k_{YN}) and τ (the time required for 80% sorbate breakthrough) [40,41]. Table 5 signified the values of these calculated parameters. The experimental data displayed good agreement with the Yoon–Nelson model that has R^2 that recorded 0.99862, 0.99881 and 0.8528 which was better than its corresponding one in Thomas model in the two cases chemisorption and physicosorption of the oil with MCM-41. The bed capacity was increased with the flow rate increased in the chemisorption of the oil with MCM-41. Fig. 11 shows the comparison of the experimental and predicted breakthrough curves obtained in the chemisorption of the oil with MCM-41 at different flow rates (0.5, 1 and 1.5 mL/min) at a constant bed height (1.5 mm) stated by the Yoon–Nelson model. From this figure, it was clear that there was less agreement than another model.

3.6. Characterizations of MCM-41 after adsorption of oil

The sample after adsorption was also characterized by FTIR, Raman and TEM as represented in Fig. 12. As a result of FTIR and Raman in Fig. 12(a) and (b), respectively, C–H stretching vibrations, a broad absorbance peak with variable wave numbers was observed. This is typical of carbon compounds containing alkane, alkene, and alkyne groups. The sharp absorbance peaks at 1,041 and 1,450 cm⁻¹ are indicative of aliphatic chains (–CH$_3$ and –CH$_2$–), and these peaks reflect the presence of alkyl chains in a compound. The peaks at approximately 3,269 cm⁻¹ indicate the C–H bonds of –CH$_2$ groups. The strong band observed at 1,619.31 cm⁻¹ is attributed to a carbonyl group; the presence of C=O bonds causing C=O stretching vibrations, which leads to absorbance peaks in these regions. The FTIR spectrum suggests the good appearance of adsorbed oil on MCM-41 surface. HRTEM image on Fig. 12(c), MCM-41 surface suffers from disorder mesoporous structure due to the oil layer adsorbed on it.

Table 5
Yoon–Nelson model parameters

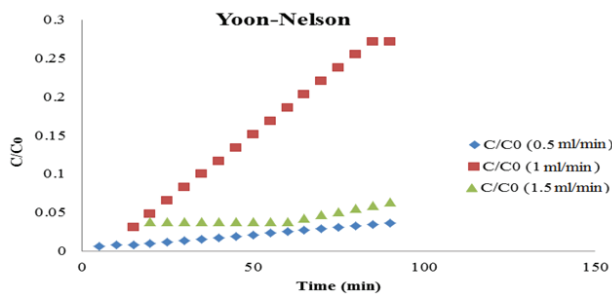| Flow (mL min–1)	KYN	R^2	τ
0.5	0.00037	0.99862	7.36748
1	0.00337	0.99881	5.3843
1.5	0.00034	0.8528	76.1364

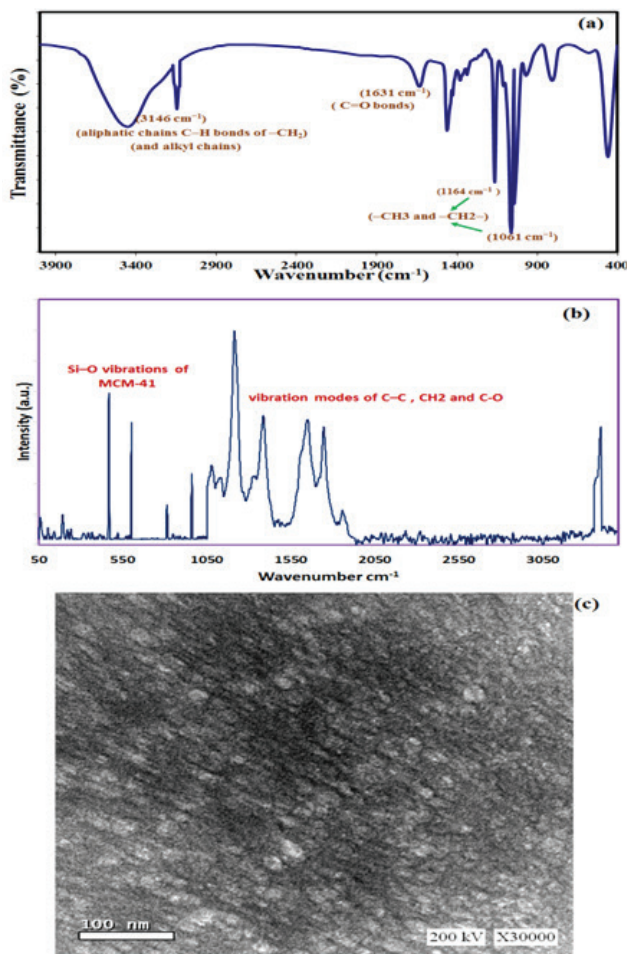Fig. 11. Yoon–Nelson model parameters for adsorption of oil on MCM-41.

Fig. 12. (a) FTIR, (b) Raman and (c) TEM image for MCM-41 after adsorption of oil.

4. Conclusion

A novel mesoporous MCM-41 for oil removal from produced water on a continuous fixed bed study was synthesized by facile, simple and cost effective method. The structure and surface morphology of prepared sample has been studied and the results reveal the formation of a pure hexagonal mesoporous structure with a high surface area of 1,022 m^2/g. The effects of flow rate (0.5, 1 and 1.5 mL/min) and bed height (0.5, 1 and 1.5 mm) on the breakthrough characteristics of the adsorption system at constant the initial oil concentration (1,000 mg/L), were determined. The maximum removal (70.26%) was achieved for a flow rate of 0.5 mL/min and a bed height of 1.5 mm. Two models Thomas and Yoon–Nelson were applied to predict the breakthrough curves and to determine the characteristic parameters useful for column design. It was clear that the Thomas model fitted well the adsorption data with a correlation coefficient (R^2) at different conditions. From the R^2 values, we suggested that the Thomas model was suitable for explaining the chemisorption of oil on MCM-41. The model employed shows that the MCM-41 was suitable for adsorption of oil using fixed bed adsorption. We found that the new modified MCM-41 was useful in water treatment and future remediation processes.

References

[1] M. Ramzi, R. Hosny, M. El-Sayed, M. Fathy, Th. Abdel Moghny, Evaluation of scale inhibitors performance under simulated flowing field conditions using dynamic tube blocking test, Int. J. Chem. Sci., 14 (1) (2016), 16–28.

[2] Z.Z. Chowdhury, S.M. Zain, R.A. Khan, K. Khalisanni, Breakthrough curve analysis for column dynamics sorption of Mn (II) ions from waste water by using Mangostana garcinia peel based granular activated carbon (GAC), J. Chem., (2013), doi:10.1155/2013/959761.

[3] R. Hosny, Th. Abdel-Moghny, M. Ramzi, S.E.M. Desouky, S.A. Shama, Preparation and characterization of natural polymer for treatment oily produced water, Int. J. Current Res., 6(3) (2014), 5413–5418.

[4] A.L. Ahmad, S. Sumathi, B.H. Hameed, Residual oil and suspended solid removal using natural adsorbents chitosan, bentonite and activated carbon: a comparative study, Chem. Eng. J., 108 (2005) 179–185.

[5] A.I. Zouboulis, A. Avranas, Treatment of oil-in-water emulsions by coagulation and dissolved-air flotation, Colloids Surf., 172 (2000) 153–161.

[6] K. Andrew, G. Graeme, G. Jeff., R.S. Brian, Flocculation and coalescence of oil-in-water poly (dimethylsiloxane) and emulsion, Colloid Interface Sci., Ideal Library 227 (2000) 390–397.

[7] R. Hosny, M. Fathy, M. Ramzi, Th. Abdel Moghny, S.E.M. Desouky, S.A. Shama, 2016, Treatment of the oily produced water (OPW) using coagulant mixtures, Egyptian Journal of Petroleum (2016) 25, 391–396.

[8] Z.Z. Chowdhury, S.M. Zain, R.A. Khan, K. Khalisanni, Process variables optimization for preparation and characterization of novel adsorbent from lignocellulosic waste, Bioresour. Technol., 7 (2012), 3732–3754.

[9] A.M. Li, Q.X. Zhang, G.C. Zhang, Adsorption of compounds from aqueous solution by a water-compatible hyper cross linked polymeric adsorbent, Chemosphere, 47 (2002) 981–989.

[10] L.B. Sun, X.-Q. Liu, H.-C. Zhou, Design and fabrication of mesoporous heterogeneous basic catalysts, Chem. Soc. Rev., 44 (15) (2015) 5092–5147.

[11] L. Martins, D. Cardoso, Influence of surfactant chain length on basic catalytic properties of Si-MCM-41, Microporous Mesoporous Mater., Nov 1; 106 (2007) 8–16.

[12] L. Martins, T.J. Bonagamba, E.R. de Azevedo, P. Bargiela, D. Cardoso, Surfactant containing Si-MCM-41: an efficient basic catalyst for the Knoevenagel condensation, Appl. Catal., A: General., 312 (2006) 77–85.

[13] A.C. Oliveira, L. Martins, D. Cardoso, Basic catalytic properties of as-synthesized molecular sieves. Microporous Mesoporous Mater., 120 (2009) 206–213.

[14] Y. Kubota, Y. Nishizaki, H. Ikeya, M. Saeki, T. Hida, S. Kawazu, M. Yoshida, H. Fujii, Y. Sugi, Organic–silicate hybrid catalysts based on various defined structures for Knoevenagel condensation, Microporous Mesoporous Mater., 70 (2004) 135–149.

[15] J. Wieslaw, The discovery of mesoporous molecular sieves from the twenty-year perspective, Chem. Soc. Rev., 42 (2013) 3663–3670.

[16] V. Meynen, P. Cool, E.F. Vansant, Verified syntheses of mesoporous materials, Microporous Mesoporous Mater., 125 (2009) 170–223.

[17] C. Perego, M. Roberto, Porous materials in catalysis: challenges for mesoporous materials, Chem. Soc. Rev., 42 (2013) 3956–3976.

[18] C.T. Kresge, M.E. Leonowicz, W.J. Roth, J.C. Vartuli, J.S. Beck, Ordered mesoporous molecular sieves synthesized by a liquid-crystal template mechanism, Nature, 359 (1992) 710–712.

[19] J.S. Beck, J.C. Vartuli, W. Jf Roth, M.E. Leonowicz, C.T. Kresge, K.D. Schmitt, C.T.W. Chu, D. Hm Olson, E.W. Sheppard, A new family of mesoporous molecular sieves prepared with liquid crystal templates, J. Am. Chem. Soc., 114 (1992) 10834–10843.

[20] I.K. Mbaraka, B.H. Shanks, Conversion of oils and fats using advanced mesoporous heterogeneous catalysts, J. Am. Oil Chem. Soc., 83 (2006) 79–91.

[21] H.Y. Huang, R.T. Yang, D. Chinn, C.L. Munson, Amine-grafted MCM-48 and silica xerogel as superior sorbents for acidic gas removal from natural gas, Ind. Eng. Chem. Res., 42 (2003) 2427–2433.

[22] J.H. Drese, S. Choi, R.P. Lively, W.J. Koros, D.J. Fauth, M.M.L. Gray, C.W. Jones, Synthesis–structure–property relationships for hyperbranchedaminosilica CO2 adsorbents, Adv. Funct. Mater., 19 (2009) 3821–3832.

[23] C. Knöfel, C. Martin, V. Hornebecq, P.L. Llewellyn, Study of carbon dioxide adsorption on mesoporous aminopropylsilane-functionalized silica and titania combining microcalorimetry and in situ infrared spectroscopy, J. Phys. Chem. C, 113 (2009) 21726–21734.

[24] M. Kruk, M. Jaroniec, Y. Sakamoto, O. Terasaki, R. Ryoo, C.H. Ko, Determination of pore size and pore wall structure of MCM-41 by using nitrogen adsorption, transmission electron microscopy, and X-ray diffraction, J. Phys. Chem. B, 104 (2000) 292–301.

[25] M. El-Sayed, M. Ramzi, R. Hosny, M. Fathy, Th. Abdel Moghny, Breakthrough curves of oil adsorption on novel amorphous carbon thin film, Water Sci. Technol., 73 (2016) 2361–2369.

[26] A. Chatterjee, S. Schiewer, Biosorption of cadmium (II) ions by citrus peels in a packed bed column: effect of process parameters and comparison of different breakthrough curve models, CLEAN-Soil Air Water, 39 (2011) 874–881.

[27] Z.Z. Chowdhury, S.M. Zain, R.A. Khan, K. Khalisanni, Batch and fixed bed adsorption studies of lead (II) cations from aqueous solutions onto granular activated carbon derived from mangostanagarcinia shell, Bioresour. Technol., 7 (2012) 2895–2915.

[28] M. Fathy, et al., Cation exchange resin nanocomposites based on multi-walled carbon nanotubes. Applied Nanoscience, 2014. 4(1): p. 103-112.

[29] H.C. Thomas, Heterogeneous ion exchange in a flowing system, J. Am. Chem. Soc., 66 (1944) 1466–1664.

[30] Y.H. Yoon, J.H. Nelson, Application of gas adsorption kinetics. I. A theoretical model for respirator cartridge service time, Am. Ind. Hyg. Assoc. J., 45 (1984) 509–516.

[31] A. Gendron-Badou, T. Coradin, J. Maquet, F. Fröhlich, J. Livage, Spectroscopic characterization of biogenic silica, J. Non-Cryst. Solids, 316 (2003) 331–337.

[32] D.V. Tsu, G. Lucovsky, B.N. Davidson, Effects of the nearest neighbors and the alloy matrix on SiH stretching vibrations in the amorphous SiO r: H (0 < r < 2) alloy system, Phys. Rev. B, 40 (1989) 1795.

[33] K. Saito, A.J. Ikushima, Effects of fluorine on structure, structural relaxation, and absorption edge in silica glass, J. Appl. Phys., 91 (2002) 4886–4890.

[34] T. Suzuki, L. Skuja, K. Kajihara, M. Hirano, T. Kamiya, H. Hosono, Electronic structure of oxygen dangling bond in glassy SiO2: the role of hyperconjugation, Phys. Rev. Lett., 90 (2003) 1–4.

[35] R.J. Prado, T.F. D'addio, M.C.A. Fantini, I. Pereyra, A.M. Flank, Annealing effects of highly homogeneous a-Si1−xCx:H, J. Non-Cryst. Solids, 330 (2003) 196–215.

[36] C.H. Giles, T.H. MacEwan, S.N. Nakhwa, D. Smith, Studies in adsorption. Part XI. A system of classification of solution adsorption isotherms, and its use in diagnosis of adsorption mechanisms and in measurement of specific surface areas of solids, J. Chem. Soc., 60 (1960) 3973–3993.

[37] C.W. Purnomo, A. Prasetya, *The study of adsorption breakthrough curves of Cr(VI) on Bagasse Fly Ash (BFA)*. In: Proceedings of the world congress on engineering and computer science, San Francisco, USA (2007).

[38] Z. Xu, J. Cai, B. Pan, Mathematically modeling fixed-bed adsorption in aqueous systems, Applied Phys. Eng., 14 (2013) 155–176.

[39] A. Ghribi, M. Chlendi, Modeling of fixed bed adsorption: application to the adsorption of an organic dye, Asian Journal of Textile, 1 (2011) 161–171.

[40] M. Fathy Th. Abdel Moghny, M.M. Abdou, Abdel-Hameed A-A. El-Bellihi, Study the adsorption of Ca (ii) and Mg (ii) on high crosslinked polystyrene divinyl benzene resin, Int. J. Modern Chem., 7 (2015) 36–44.

[41] M. Fathy, M.A. Mousa, Th. Abdel Moghny, M.M.A. Abdel-Hameed, A-A. ElBellihi, A.E. Awadallah, Synthesis and characterization of cellulose nanoparticles obtained from rice straw waste, Int. J. Modern Organic Chem., 4 (2015) 56–61.